Title

Self-Assembled Framework Formed During Lithiation of SnS2 Nanoplates Revealed by in Situ Electron Microscopy

Journal

Accounts of Chemical Research, 50(7)

ISSN

0001-4842

Authors

Yin, Kuibo
Zhang, Minghao
Hood, Zachary D
et al.

Publication Date

2017-07-18

DOI

10.1021/acs.accounts.7b00086

Peer reviewed

ACCOUNTS of chemical research

Article

pubs.acs.org/accounts

Self-Assembled Framework Formed During Lithiation of SnS_2 Nanoplates Revealed by in Situ Electron Microscopy

Published as part of the Accounts of Chemical Research special issue "Direct Visualization of Chemical and Self-Assembly Processes with Transmission Electron Microscopy".

Kuibo Yin,[†,‡,#] Minghao Zhang,[‡,⊥,#] Zachary D. Hood,[‡,§,#] Jie Pan,[∥] Ying Shirley Meng,[⊥] and Miaofang Chi*[,‡]

[†]Key Lab of MEMS of Ministry of Education, Southeast University, Nanjing 210096, China

[‡]Center for Nanophase Materials Sciences, Oak Ridge National Laboratory, Oak Ridge, Tennessee 37831, United States

[§]School of Chemistry and Biochemistry, Georgia Institute of Technology, Atlanta, Georgia 30332, United States

[∥]Department of Materials Science and Engineering, University of Kentucky, Lexington, Kentucky 40506, United States

[⊥]Department of NanoEngineering, University of California at San Diego, La Jolla, California 92093, United States

Supporting Information

CONSPECTUS: Lithium-ion batteries (LIBs) commercially dominate portable energy storage and have been extended to hybrid/electric vehicles by utilizing electrode materials with enhanced energy density. However, the energy density and cycling life of LIBs must extend beyond the current reach of commercial electrodes to meet the performance requirements for transportation applications. Carbon-based anodes, serving as the main negative electrodes in LIBs, have an intrinsic capacity limitation due to the intercalation mechanism. Some nanostructured carbon materials offer very interesting reversible capacities and can be considered as future anode materials. However, their fabrication processes are often complicated and expensive. Theoretically, using a lithium metal anode is the best way of delivering high energy density due to its largest theoretical capacity of more than 3800 mAh g^{-1}; however, lithium metal is highly reactive with liquid electrolytes. Alternative anodes are being explored, including other lithium-reactive metals, such as Si, Ge, Zn, V, and so forth. These metals react reversibly with a large amount of Li per formula unit to form lithium−metal alloys, rendering these materials promising candidates for next-generation LIBs with high energy density. Though, most of these pure metallic anodes experience large volume changes during lithiation and delithiation processes that often results in cracking of the anode material and a loss electrical contact between the particles.

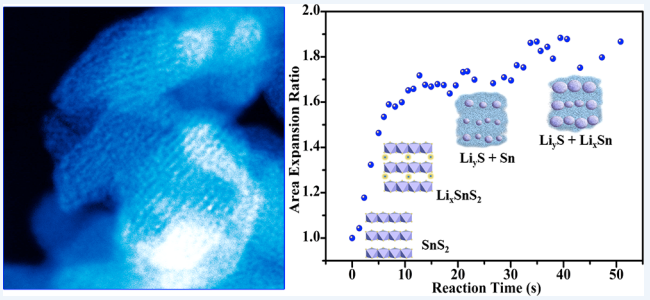

Nanosized metal sulfides were recently found to possess better cycling stability and larger reversible capacities over pure metals. Further improvements and developments of metal sulfide-based anodes rely on a fundamental understanding of their electrochemical cycling mechanisms. Not only must the specific electrochemical reactions be correctly identified, but also the microstructural evolution upon electrochemical cycling, which often dictates the cyclability and stability of nanomaterials in batteries, must be clearly understood. Probing these dynamic evolution processes, i.e. the lithiation reactions and morphology evolutions, are often challenging. It requires both high-resolution chemical analysis and microstructural identification. In situ transmission electron microscopy (TEM) coupled with electron energy loss spectroscopy (EELS) has recently been raised as one of the most powerful techniques for monitoring electrochemical processes in anode materials for LIBs.

In this work, we focus on elucidating the origin of the structural stability of SnS_2 during electrochemical cycling by revealing the microstructural evolution of SnS_2 upon lithiation using in situ TEM. Crystalline SnS_2 was observed to undergo a two-step reaction after the initial lithium intercalation: (1) irreversible formation of metallic tin and amorphous lithium sulfide and (2) reversible transformation of metallic tin to Li−Sn alloys, which is determined to be the rate-determining step. More interestingly, it was discovered that a self-assembled composite framework formed during the irreversible conversion reaction, which has not been previously reported. Crystalline Sn nanoparticles are well arranged within an amorphous Li_2S "matrix" in this self-assembled framework. This nanoscale framework confines the locations of individual Sn nanoparticles and prevents particle agglomeration during the subsequent cycling processes, therefore providing desired structural tolerance and warranting a sufficient

continued...

Received: February 12, 2017

DOI: 10.1021/acs.accounts.7b00086
Acc. Chem. Res. XXXX, XXX, XXX−XXX

electron pathway. Our results not only explain the outstanding cycling stability of SnS_2 over metallic tin anodes, but also provide important mechanistic insights into the design of high-performance electrodes for next-generation LIBs through the integration of a unique nanoframework.

INTRODUCTION

Lithium-ion batteries (LIBs) represent one of the most promising energy storage systems for most of today's portable electronic devices and electric vehicles due to their high energy and power density coupled with long cycle life. The LIB industry is progressively looking for new anode materials (rather than conventional graphitic anodes) with increased specific capacities, fast charging/discharging ability and superior safety for energy storage for use in the next generation of more powerful rechargeable batteries.[1−6] Tin serves as one of the best solutions available because of its high theoretical capacity of 990 mAh g^{-1}.[7−9] Tin anodes, however, suffer from volume changes during battery cycling similar to other metallic materials such as germanium and aluminum, which inherently results in anodic degradation.[10−12] To overcome this problem, many Sn-based materials, such as composites and intermetallic compounds, have been studied, some of which have shown promise for use in LIBs. Disordered carbon,[13] graphite,[14] single-walled carbon nanotubes (SWNTs),[15] multiwalled carbon nanotubes (MWNTs),[16] TiO_2 nanotubes,[17] and semiamorphous copper[18] were determined as effective secondary phases to accommodate the excessive volume changes during the charging/discharging cycles. However, the synthesis of these composite materials requires more complicated and difficult industrial processes, which limits the feasibility of implementing such anodes into the LIB technology. Tin disulfide (SnS_2) possesses better cycling stability and larger reversible capacities over metallic tin, which renders this material as one of the most promising, high-performance anodes for LIBs.

In previous reports, SnS_2 anodes have shown good cycling stability between 0 and 2.5 V.[19−22] For example, ultrathin SnS_2 nanoplates (with the thickness of ∼2 nm) showed an excellent capacity retention of over 90% after 50 cycles under at a high rate of 1 C.[21] In comparison, a metallic tin electrode cannot be cycled more than a few times due to premature degradation derived from excessive volumetric changes. For SnS_2, it is believed that multiple phases form during the initial irreversible reactions, including tin metal.[23,24] However, it is unknown how these phases spatially distribute during electrochemical cycling and what is the primary reason for the enhanced structural stability of SnS_2 compared to that of pristine Sn anode. Our work primarily focuses on elucidating the origin of structural stability in SnS_2 upon cycling by revealing the dynamic microstructural evolution during the lithiation processes and linking the observed stability to the electrochemical performance.

To capture both the chemical dynamics and the intermediate states involved in the lithiation process of SnS_2, in situ investigations provide direct observations and reliable data sets compared to conventional ex situ characterization methods. Many in situ characterization methods can be used to study the structural evolution of the electrode materials during battery operation, such as X-ray diffraction (XRD), X-ray absorption spectroscopy (XAS), scanning electron microscopy (SEM) imaging, and transmission electron microscopy (TEM).[25−27] Among them, in situ TEM provides insight related to both microstructural and chemical evolutions with a superior spatial resolution.[28−30] Recently, in situ TEM techniques have been explored for monitoring the electrochemical reaction of nanostructures in a variety of novel lithium battery electrode materials.[31−33] Huang et al. observed that Sn particles were formed and randomly distributed in the Li_2O matrix during the conversion process.[32] Further lithiation triggers alloying reactions between Sn particles and Li, inducing large volume expansions. Recently, Gao et al. studied the in situ lithiation of SnS_2 anodes in the intercalation range with Li_xSnS_2, $x \sim 1$. Because a limited amount of lithium was inserted into the structure, no obvious volume expansion was observed in this work.[33]

Here, the lithiation mechanism regarding both the chemical and structural evolutions of SnS_2 nanoplates is explored using in situ TEM. We focus on the conversion and alloy reactions, which were found to be a major contributor to the reversible capacity. Not only a two-step reaction process was revealed, but we also discovered a fascinating, spontaneously formed, self-assembling nanocomposite framework with spatially and periodically aligned tin nanoparticles buried in the lithium sulfide amorphous matrix. This framework provides adequate room to accommodate the volume expansion of tin during lithiation while ensuring enhanced contact among the active materials. As a result, adequate mechanical and structural stability and high electric and ion conduction are realized. Our results therefore elucidate the superior electrochemical performances of SnS_2 anode compared to that of Sn metal. We believe that the formation of such architecture happens in most metallic sulfides with a layered structure. Our results are expected to promote the mechanistic understanding of the electrochemical processes in materials with a similar crystal structure.

EXPERIMENTAL SECTION

Synthesis, Sample Preparation, and Experimental Setup

Laterally confined 2D SnS_2 nanoplates were synthesized using solvothermal methods.[21] The in situ experiments were performed using a biasing holder (Nanofactory) that allows a nanoscale electrochemical cell to generate within the TEM. As shown in Supporting Information Figure S1, the nanosized electrochemical device consists of two essential components which can be moved via piezo control: (1) a piece of lithium metal coated with a thin layer of lithium oxide acts as the lithium source and (2) a half lacey carbon TEM grid coated with multilayer (2−3 layers) graphene on which SnS_2 plates are dispersed (Figure S1). All of the components were loaded onto the holder in an argon-filled glovebag and then transferred into the TEM column. During transferring the holder into the TEM column, the lithium metal was intentionally exposed to air (∼2 s) to form a thin passivation layer of lithium oxides on the surface that not only prevents direct chemical reaction and acts but also as a solid electrolyte layer. Graphene sheets serve an important role in this experiment: ensuring the ion and electron conduction in between SnS_2 nanoplates and providing improved time range for in situ observation. Instead of only one of two particles which are directly in contact with lithium oxide in conventional in situ lithiation configurations, this configuration allows each nanoparticle on the carbon grid to be chosen for investigation. As a result, a complete morphology evolution, from the beginning to the end of the lithiation process of single nanoparticle, can be obtained. During all in situ experiments, a potential of −2.5 V was applied to the SnS_2 electrode with respect to the Li electrode to drive the lithiation process.

DOI: 10.1021/acs.accounts.7b00086
Acc. Chem. Res. XXXX, XXX, XXX−XXX

TEM Characterization

TEM characterizations were carried out on an aberration-corrected FEI Titan 80/300 microscope equipped with a Gatan Quantum ER electron energy loss spectrometer (EELS). Area expansion ratios were measured by averaging the 2D projection of multiple particles at different reaction stages in respect to that of their pristine stage. Theoretical estimation of the area expansion ratio for different reaction stages are calculated based on the change in the unit cell volume of each related material from the ICSD database. The Z-contrast images presented in this work were acquired with a convergence semiangle of 30 mrad and an inner collection semiangle of 60 mrad at 300 kV. EELS was acquired spectra were acquired with a collection semiangle of 50 mrad, and each spectrum presented in this paper is a sum of 40 spectra.

INITIAL LITHIATION OF SnS_2 OCCURS IN A TWO-STEP MECHANISM

The lithiation process of single SnS_2 grains was recorded using in situ TEM imaging. Figure 1 shows time-lapse images of two grains that physically overlap each other during their lithiation (also see the corresponding movie in the Supporting Information). In spite of their overlapping, their diffraction contrast allows for differentiation of the grains throughout the entire lithiation process. Figure 1A is a TEM image of the

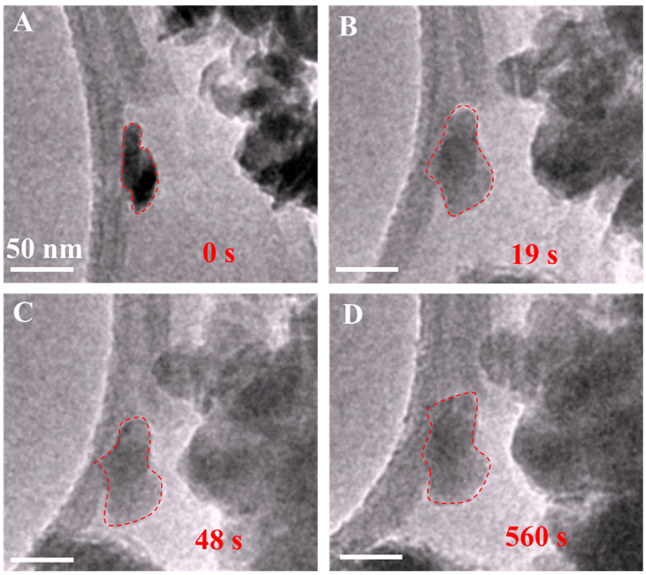

Figure 1. Initial lithiation process of SnS_2. Time-series showing the volume expansion of SnS_2 nanoplates (indicated by the red dashed lines) supported on a graphene-coated lacey carbon film.

electrode before the reaction with lithium. The SnS_2 nanoparticles studied in this work exhibit plate-like morphology preferentially grown along [100] and [010]. As SnS_2 adopts a layered structured with van der Waals interaction between the layers, the thickness of nanoplate is expected to experience a larger volume change during lithiation. The nanoplates which sit edge-on the grid, i.e., those with {001} surface planes parallel to the electron beam, are chosen for detailed analysis. Before lithiation, the SnS_2 nanoplates typically have a 30−40 nm lateral thickness and ∼80 nm planar width. Figure 1B marks the start of the reaction process, where a potential of −2.5 V was applied to the SnS_2 electrode; the TEM image shows instant volume expansion with vaguely seen nanoinclusions with a darker contrast compared to the matrix. Figure 1C and D presents TEM images of the reaction dynamics as these crystals grow larger (from ∼40 to ∼50 nm), and the nanoinclusions remain inside the grain. As the reaction propagates, the overall size of each grain increases, and the TEM image contrast changes from a typical diffraction contrast of single crystals to a gray, mostly featureless contrast, which indicates that clear phase transformations occur in the SnS_2

The dynamic volume expansion of individual SnS_2 nanoplates revealed by in situ TEM was further evaluated to elucidate potential reaction processes, based on the fact the distinctive lithiation reactions often introduce different volume changes in materials. The area expansion ratio, which is defined as the 2D projected area of individual nanoplates in TEM images relative to those at their pristine states, was used to evaluate volume changes in SnS_2 nanoplates. The shape and size of individual particles at different lithiation stages were identified and estimated by using ImageJ. Figure 2 shows the area expansion ratio evolution as a

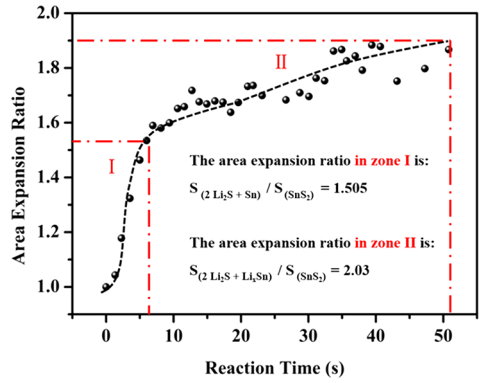

Figure 2. Area expansion ratio of the SnS_2 nanocrystals as a function of reaction time. Two different reaction speeds can be obtained. The black dashed curve shows the average trend of changes in the area expansion ratio.

function of lithiation time of the particles delineated in Figure 1. Since these SnS_2 nanoplates sit edge-on the grid, the area expansion mainly represents the increase of the space between (001) planes. In previous studies, the volume increases slowly with a Li content $x < 1$ in Li_xSnS_2.[23] Our experimental results show that the volume increases relatively rapidly with the lithiation time during the initial stage, indicating the rapid lithiation during the initial stage in our experiment. This rapid lithiation should be attributed to the difference in applied voltages. In our case, a relatively large voltage bias (2.5 V) was applied between two electrodes, which possibly suppressed the initial intercalation stage and directly triggered the conversion reaction with a huge volume expansion rate. The same phenomenon has also been reported by Huang et al.[32] Interestingly, two different reaction zones are clearly identified according to the changing rate of the area expansion ratio. In Zone I, the area expansion ratio for grains increases greatly from 1.0 to 1.5 within only a few seconds. On the other hand, the area expansion ratio in Zone II increases to 1.9 at a much slower rate. Although the size of the grains increase during the entire lithiation process, the different rates for area expansion ratios in these zones clearly indicate that two different reaction processes with different kinetics occur during lithiation.

It is generally acknowledged that two different reactions occur when a SnS_2 electrode is cycled versus a metallic lithium electrode.[34] The first step, which happens around 0.7 V vs Li^+/Li,

DOI: 10.1021/acs.accounts.7b00086
Acc. Chem. Res. XXXX, XXX, XXX−XXX

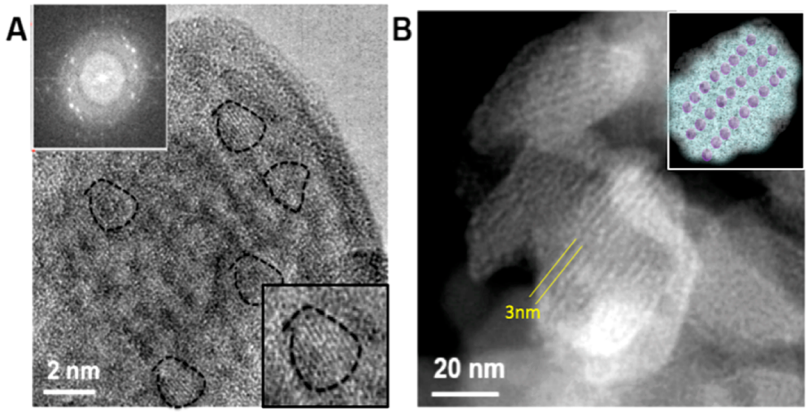

Figure 3. Characterization of lithiated SnS_2 nanoplates. (A) A typical HRTEM image of lithiated SnS_2 nanoplates composed of amorphous matrix and crystalline nanoparticles. The top inset are the corresponding FFT pattern from the entire particle and the bottom inset shows an individual crystalline nanoparticle with lattice fringes (B) STEM-HAADF image of a lithiated SnS_2 cluster distributed in {001} planes with a planar spacing of ∼3 nm. The inset is a schematic of the newly formed unique nanoarchitecture with aligned crystalline particles dispersed into a light-contrasted amorphous matrix.

represents the formation of metallic tin and lithium sulfide by the following reaction:

$$SnS_2 + 4Li \rightarrow Sn + 2Li_2S \quad (1)$$

It is worth noting that this reaction is irreversible.[23] Thus, the subsequent charging and discharging are related to the reversible phase transformation of metallic tin and lithium tin alloys:

$$Sn + xLi \leftrightarrow Li_xSn \quad (2)$$

As expected, the area expansion ratio changes for the two different zones, which can be related to the reactions outlined above. The change in the area expansion ratio of reaction 1 can be estimated to be 1.505 based on the estimation of crystalline structural changes from SnS_2 to Li_2S, which is comparable to the experimental result of ∼1.5 in Zone I. In Zone II, the area expansion ratio gradually increases from 1.5 to 1.9, approaching the estimation (2.03) based on the chemical reaction in eq 2. Therefore, the two-step reaction mechanism of tin disulfide electrode, as described above, is confirmed by our area expansion ratio analysis using the in situ TEM observation. Additionally, these results demonstrate that the irreversible formation of metallic tin occurs much faster when compared to the transformation of tin to different lithium tin alloys, which compromises the rate performance of the SnS_2 electrode.

It is important to point out that this two-step reaction mechanism may not be present in other metal sulfides though they may also hold a layered structure. For example, during the lithiation of molybdenum disulfide, lithium ions reversibly intercalate into the vacant sites in between layers of MoS_2 upon applying a voltage at 3 to 1.1 V vs Li/Li^+, forming crystalline Li_xMoS_2.[35] Further lithiation triggers an irreversible conversion reaction of Li_xMoS_2 to Li_2S and Mo in the system. The lithium−sulfur redox couple dominates the subsequent cycling process of MoS_2. Therefore, the major difference in the lithiation mechanism between MoS_2 and SnS_2 lies in the responsible reactions that eventually contribute to the subsequent charging and discharging processes, where the Li−S reaction dominates in MoS_2 while the Sn−Li reaction prevails in SnS_2. Such different reaction mechanisms in sulfides with similar layered structures demonstrate the importance of a precise understanding of the reaction mechanism in individual materials.

STRUCTURE AND CHEMICAL EVOLUTION DURING THE INITIAL LITHIATION PROCESS

Figure 3 shows a more detailed structure and phase characterization of the lithiated SnS_2 nanoplates. After lithiation, the SnS_2 contain small crystalline nanoparticles (as represented by dashed circles in Figure 3A) embedded in an amorphous matrix. The corresponding fast Fourier transform (FFT) pattern clearly shows the mixture of both crystalline and amorphous phases in the sample. The crystalline nanoparticles exhibit a brighter contrast in high-angle annular dark field (HAADF) image (Figure 3B), which should correspond to Sn-containing compounds. After multiple potential Li−Sn compounds have been considered, the diffraction spots match both the tetragonal tin and a lithium tin, $Li_{13}Sn_5$, alloy. Closer examination of the HAADF images shows a very fascinating phenomenon. Many lithiated grains show spatially aligned arrays of these nanoparticles within the amorphous matrix, forming an interesting nanoarchitecture composed of an aligned nanoinclusion-amorphous matrix. In fact, if the specimen is tilted, many nanoparticles show the same planar arrangement, which indicates that the nanoparticles are aligned as layers in the amorphous matrix. Since the end products include Li_2S and Li_xSn, all the evidence, including HAADF image contrast and diffraction spacing, show that the amorphous matrix should be Li_2S while the crystalline nanoparticles should be Li_xSn. This nanocomposite configuration with nanoparticle self-assembled in amorphous matrix has not been previously reported. In such a framework, Li_xSn nanoparticles hold a uniform grain size (∼3 nm) and each exhibits the same lattice fringes as shown in Figure 3A in TEM imaging. The nanoparticle layers are homogeneously distributed with a planar spacing of ∼3 nm. A schematic is presented as an inset in Figure 3B. Taking advantage of the in situ experiment, the direction in which the nanoparticles are aligned can be inferred by corroborating the initial orientation of the SnS_2 grains. It was found that that the nanoarchitecture of each particle is closely related to the initial grain orientation of SnS_2 nanoplates, with their {001} plane parallel to the electron beam. These results indicate that the inclusion nanoparticles are distributed at the {001} planes of initial SnS_2 nanoplates. Such well-aligned spatial distribution of Li_xSn demonstrates that the lithiation reactions happen locally in the crystalline structure of SnS_2, representing an intercalation-like behavior. As a result, a layered framework is preserved.

DOI: 10.1021/acs.accounts.7b00086
Acc. Chem. Res. XXXX, XXX, XXX−XXX

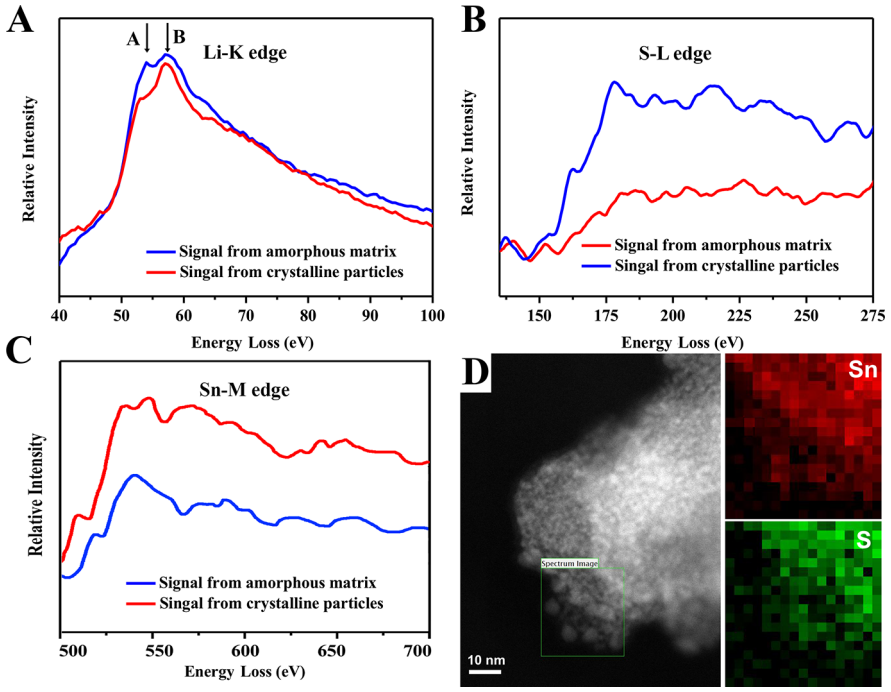

Figure 4. (A) Li K-edge, (B) S L-edge, and (C) Sn M-edge results for SnS_2 nanocrystals lithiation reaction in different phases. (D) EELS mapping results showing that the formed particles are Sn-enriched and the amorphous phase is S-enriched.

Electron energy loss spectroscopy (EELS) was performed to confirm chemical compositions of the newly formed phases observed in STEM imaging for lithiated SnS_2 (Figure 4). A probe size of ~0.5 nm was used so that the spectra can be collected locally from the amorphous matrix and crystalline nanoparticles, respectively. The spectra in Figure 4 were acquired using the same experimental condition as the initial SnS_2 grain where the same thickness of the analyzed region can be assumed. The concentration of each element in the crystalline nanoparticle and amorphous matrix can therefore directly be compared using raw spectra. As shown in Figure 4A, both the amorphous matrix and the crystalline nanoparticles contain a relatively greater amount of lithium, as expected. The amorphous matrix mostly consists of sulfur while the crystalline nanoparticles largely consist of tin (Figure 4B and C). EELS quantification was performed by using 20 spectra from different regions of the amorphous and crystalline phases, respectively. It was estimated that the atomic concentration of lithium in the amorphous matrix is around 1.9 ± 0.3 relative to each S atom, which corresponds to that of Li_2S. It is noticeable that the spectra from the amorphous matrix also contain some Sn signal, which is possibly due to delocalization of the EELS signal for Sn and/or specimen drift. The quantification of Li:Sn atomic ratio for the nanocrystalline particles, however, leads to a relatively large error bar, which is $\sim 2.5 \pm 1.0$. The potential reason for such a large error bar can be attributed to the embedment of Li_xSn nanoparticles in the Li_2S matrix. Therefore, the spectra from the Li_xSn nanoparticles include the signal from both the nanoparticle and its surrounding Li_2S matrix. Consequently, a reliable quantification of the elemental stoichiometry in Li_xSn cannot be reached merely based on EELS spectra. It needs to be noted that the fine structure of Li K-edges shows clear differences in the spectra of the nanoparticle compared to that of matrix (Figure 4A). Although both Li K-edge spectra contain two major peaks that are labeled as peak "A" and "B" in Figure 4A, their intensity ratio and positions are clearly distinctive in the two spectra. These fine structure differences suggest distinctive bonding configurations of Li with its neighbor ions in the matrix and nanoparticle, indicating the chemical bonding of Li with Sn in the nanoparticles. The FFT of TEM images (Figure 3A) suggest that the nanoparticle can potentially be either metallic Sn or $Li_{13}Sn_5$. The EELS Li K-edge fine structures therefore refine the phase of nanoparticles to be $Li_{13}Sn_5$.

EELS mapping results in Figure 4D further support a phase separation with a consistent chemistry as revealed by individual spectra. In order to obtain enough chemical signal from EELS, we scanned a small portion of surface area for extended time and induced nanoparticle agglomeration at grain surfaces. This area was chosen to perform elemental mapping to further obtain chemical information from grain matrix and nanoparticles. The spatial association of Sn with the nanoparticles is clearly revealed, and S is present in both nanoparticles and matrix as evidenced by EELS spectra. EELS analysis combined with (S)TEM imaging therefore confirms the formation of a self-assembled composite framework that consists of crystalline $Li_{13}Sn_5$ spherical nanoparticles dispersed in the amorphous Li_2S matrix after the initial lithiation process of the SnS_2 anode material.

INFLUENCE OF THE SELF-ASSEMBLED FRAMEWORK ON ELECTROCHEMICAL PERFORMANCE

The present (S)TEM imaging and EELS analysis provide important mechanistic insight as to the structural evolution and the spatial correlation between newly formed crystalline Li_xSn nanoparticles and an amorphous Li_yS matrix upon the lithiation of the SnS_2 nanocrystals. Lithium diffusion into metallic tin nanoparticles within the lithium sulfide matrix requires lithium transport through both the lithium sulfide network and the tin nanoparticles, which presents a longer diffusion distance for lithium ion transport.[36,37] As a result, the first process of amorphization and nucleation of Li_xSnS_2 is much faster. It can also be reasonably inferred that the spatial distribution between

DOI: 10.1021/acs.accounts.7b00086
Acc. Chem. Res. XXXX, XXX, XXX−XXX

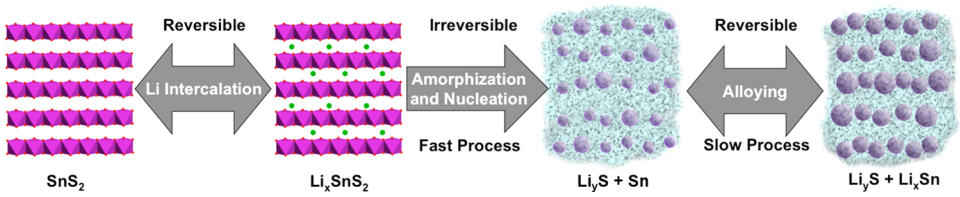

Figure 5. Schematic representation of the lithiation reaction for SnS_2 nanocrystals. Pink, Sn; red, S; green, Li; blue matrix, Li_yS; purple, Li_xSn.

the newly formed Li_xSn and Li_2S phases would influence lithium diffusion to a large extent, which impacts the overall charging and discharging rates.

We summarize the structural evolution of SnS_2 upon lithiation by the schematic shown in Figure 5, which is featured by the initial lithium intercalation, amorphization, nucleation, and growth of crystallized Li_xSn from the amorphous Li_yS matrix. At the beginning, lithium ions are intercalated into the vacant sites throughout the layered structure of SnS_2, resulting in an elongation of the ⟨001⟩ direction in the crystal lattice. This elongation has been predicted by first-principles calculations which implies that lithium prefers to occupy the vacancy sites between layers.[36] After decreasing the voltage of the anode to ~0.7 V, more lithium ions diffuse into the Li_xSn crystals, triggering a conversion reaction in the system. Metallic tin nucleates from the crystals and the whole crystal starts transforming to an amorphous lithium sulfide phase. According to the theoretical prediction,[36] the net charge on tin in Li_xSnS_2 gradually reduces during the conversion reaction and reaches about 0 at $x = 3$, which indicates the metallic tin is generated. The newly formed framework not only preserves the layered structure of the pristine SnS_2 to a certain extent, but also confines the location of the growing nanoparticles so that metallic tin is homogeneously dispersed between the fringes of the framework. In the last step, lithium ions reversibly alloy with the formed metallic tin nanoparticles. This reversible alloy reaction dominates the system in the following charging/discharging processes.

This self-assembled composite framework of spherical Li_xSn crystalline nanoparticles dispersed in the amorphous Li_yS fringes has several advantages. First, the well-arranged amorphous Li_yS fringes act as a buffer to relax the strain of the spherical Li_xSn crystalline nanoparticles. Simultaneously, the structural and electrochemical stability can be preserved to a large extent. Second, as amorphous Li_yS is an electronic insulator, the connectivity of the crystalline Li_xSn particles largely determine the electrical conductivity as well as the charging and discharging rates of the battery. Third, crystalline Li_xSn nanoparticles are well arranged between amorphous Li_yS fringes in this self-assembled framework, which prevents agglomeration of the crystalline Li_xSn nanoparticles during cycling. Therefore, lithium diffusion in this system is favorable compared to the materials with random distribution of Li_yS and Li_xSn. Overall, this unique framework enhances both structural stability and electronic conductivity, which explains the superior electrochemical performance of SnS_2 over pristine Sn anodes.

CONCLUSIONS

In summary, we have elucidated the origin of the structural stability of SnS_2 nanoplates by simultaneously probing and correlating the microstructural evolution with lithiation reactions in situ using S/TEM imaging and EELS. SnS_2 nanoplates undergo a two-step reaction during the initial lithium intercalation: (1) irreversible formation of metallic tin and amorphous lithium sulfide and (2) reversible transformation of metallic tin to Li−Sn alloys. More importantly, a self-assembled framework that is believed to be responsible to the high structural stability of SnS_2 upon cycling was discovered. This framework is formed at the initial lithiation stage with metallic tin particles well aligning within amorphous lithium sulfide matrix. The sulfide matrix acts as a buffer to relax the large strain formation due to the volume expansion of the tin nanoparticles in the second step and the following cycling processes. The well dispersed and spatially confined tin particles improve the connectivity of the Li_xSn nanoparticles, which determines the electrical conductivity of the entire system. By quantifying the volume change of single SnS_2 nanoplates, which is directly associated with the amount of lithium insertion, the second reaction step, i.e., the irreversible formation of metallic tin from SnS_2, was revealed to be much faster compared to the first step reaction, i.e., the transformation of tin to different lithium tin alloys, compromising the desirable rate performance of SnS_2. Our work highlights the importance of correlatively investigating evolving microstructures with electrochemical reactions during electrochemical cycling. Not only the phases of reaction and intermediate products but also the morphological correlations and relative spatial locations of coexisting phases are crucial to the cycling performance. Forming a nanoframework with active nanoparticles spatially aligned in an amorphous matrix may serve as a strategy to not only design electrodes for enhanced structural stability and mechanical compatibility while maintaining good ionic conductivity, but also to the synthesis of new nanocomposites with unique architectures.

ASSOCIATED CONTENT

Supporting Information

The Supporting Information is available free of charge on the ACS Publications website at DOI: 10.1021/acs.accounts.7b00086.

Detailed experimental procedures, schematic of in situ TEM setup for the lithiation process, and analysis methods (PDF)

Representative video of the structural stability of SnS_2 (ZIP)

AUTHOR INFORMATION

Corresponding Author

*E-mail: chim@ornl.gov.

ORCID

Ying Shirley Meng: 0000-0001-8936-8845

Miaofang Chi: 0000-0003-0764-1567

Author Contributions

#K.Y., M.Z., and Z.D.H contributed equally to this work.

Notes

This manuscript has been authored by UT-Battelle, LLC under Contract No. DE-AC05-00OR22725 with the U.S. Department of Energy. The United States Government retains and the

DOI: 10.1021/acs.accounts.7b00086
Acc. Chem. Res. XXXX, XXX, XXX−XXX

The authors declare no competing financial interest.

Biographies

Kuibo Yin received his B.S. in Materials Science from Nanjing University in 2008. He is currently an associate professor of electronic science and engineering at Southeast University in China. His research interests lie in the characterization of energy storage materials and novel 2D materials by in situ transmission electron microscope.

Minghao Zhang received his B.S. in Physics from Nankai University in 2009 and M.S. in Materials Physics and Chemistry from Chinese Academy of Sciences in 2012. He is currently a Ph.D. candidate in the Laboratory for Energy Storage and Conversion (LESC) at University of California, San Diego. His research interests include advanced lithium-ion and post-lithium-ion batteries based on the novel type of electrode materials.

Zachary D. Hood received his B.S. in chemistry with biochemistry and a B.A. in German from Wake Forest University in 2013. He is currently a Ph.D. candidate at Georgia Tech. His research interest includes the development of materials for biomedical and energy-related applications.

Jie Pan received his Ph.D. in Materials Science and Engineering from University of Kentucky and B.S. in Applied Physics in Jinan University, Guangzhou, China. He is currently a postdoctoral researcher at the National Renewable Energy Laboratory in Golden, Colorado. His research interest includes the development of energy materials through high throughput computational materials design.

Ying Shirley Meng received her Ph.D. in Advanced Materials for Micro & Nano Systems from the Singapore-MIT Alliance in 2005. She is currently an Associate Professor in the Department of NanoEngineering at University of California, San Diego. She is the principal investigator of the Laboratory for Energy Storage and Conversion. She is the founding Director of Sustainable Power and Energy Center (SPEC), focusing on making breakthroughs in distributed energy generation, storage, and the accompanying power-management systems. She received 2011 NSF Early Career Award and 2016 ECS Charles Tobias Award.

Miaofang Chi is a research scientist at ORNL. She received her Ph.D. in Materials Science and Engineering from University of California, Davis in 2008, and was a research fellow at Lawrence Livermore National Laboratory (2006–2008). She received the 2016 Burton Medal from the Microscopy Society of America, the 2015 ORNL Director's Award and the Early Career Research Award, and the 2007 MAS Distinguished Scholar Award. Her research interest is in the development and application of in situ and functional STEM imaging and spectroscopy for energy materials.

■ ACKNOWLEDGMENTS

This research was sponsored by the Materials Sciences and Engineering Division of the U.S. Department of Energy (DOE), Office of Basic Energy Sciences (BES), and was performed at the Center for Nanophase Materials Sciences (CNMS) at Oak Ridge National Laboratory (ORNL), which is a DOE Office of Science User Facility. K.Y. acknowledges the support from the Natural Science Foundation of China and Jiangsu Province (Nos. 11674052 and BK2012123). Z.D.H. gratefully acknowledges a Graduate Research Fellowship from the National Science Foundation (No. DGE-1148903) and the Georgia Tech-ORNL Fellowship.

■ REFERENCES

(1) Nishi, Y. Lithium ion secondary batteries; past 10 years and the future. *J. Power Sources* **2001**, *100*, 101–106.
(2) Kojima, T.; Ishizu, T.; Horiba, T.; Yoshikawa, M. Development of lithium-ion battery for fuel cell hybrid electric vehicle application. *J. Power Sources* **2009**, *189*, 859–863.
(3) Gitzendanner, R.; Puglia, F.; Martin, C.; Carmen, D.; Jones, E.; Eaves, S. High power and high energy lithium-ion batteries for underwater applications. *J. Power Sources* **2004**, *136*, 416–418.
(4) Tarascon, J. M.; Armand, M. Review article issues and challenges facing rechargeable lithium batteries. *Nature* **2001**, *414*, 359–367.
(5) Shao-Horn, Y.; Croguennec, L.; Delmas, C.; Nelson, E. C.; O'Keefe, M. A. Atomic resolution of lithium ions in $LiCoO_2$. *Nat. Mater.* **2003**, *2*, 464–467.
(6) Kang, B.; Ceder, G. Battery materials for ultrafast charging and discharging. *Nature* **2009**, *458*, 190–193.
(7) Arrebola, J. C.; Caballero, A.; Camer, J. L. G.; Hernen, L.; Morales, J.; Sanchez, L. Combining 5 V $LiNi_{0.5}Mn_{1.5}O_4$ spinel and Si nanoparticles for advanced Li-ion batteries. *Electrochem. Commun.* **2009**, *11*, 1061–1064.
(8) Lindsay, M. J.; Wang, G. X.; Liu, H. K. Al-based anode materials for Li-ion batteries. *J. Power Sources* **2003**, *119*, 84–87.
(9) Winter, M.; Besenhard, J. O. Electrochemical lithiation of tin and tin-based intermetallics and composites. *Electrochim. Acta* **1999**, *45*, 31–50.
(10) Cui, Y. H.; Xue, M. Z.; Wang, X. L.; Hu, K.; Fu, Z. W. InP as new anode material for lithium ion batteries. *Electrochem. Commun.* **2009**, *11*, 1045–1047.
(11) Chan, C. K.; Zhang, X. F.; Cui, Y. High capacity Li ion battery anodes using Ge nanowires. *Nano Lett.* **2008**, *8*, 307–309.
(12) Tatsuma, T.; Taguchi, M.; Oyama, N. Inhibition effect of covalently cross-linked gel electrolytes on lithium dendrite formation. *Electrochim. Acta* **2001**, *46*, 1201–1205.
(13) Lee, S. H.; Mathews, M.; Toghiani, H.; Wipf, D. O.; Pittman, C. U., Jr. Fabrication of carbon-encapsulated mono- and bimetallic (Sn and Sn/Sb alloy) nanorods. potential lithium-ion battery anode materials. *Chem. Mater.* **2009**, *21*, 2306–2314.
(14) Park, J.; Eom, J. Y.; Kwon, H. Fabrication of Sn–C composite electrodes by electrodeposition and their cycle performance for Li-ion batteries. *Electrochem. Commun.* **2009**, *11*, 596–598.
(15) Zheng, J. W.; Nai, S. M. L.; Ng, M. F.; Wu, P.; Wei, J.; Gupta, M. Supramolecular chirality and chiral inversion of tetraphenylsulfonato porphyrin assemblies on optically active polylysine. *J. Phys. Chem. C* **2009**, *113*, 14015–14020.
(16) Chen, W. X.; Lee, J. Y.; Liu, Z. The nanocomposites of carbon nanotube with Sb and SnSb0.5 as Li-ion battery anodes. *Carbon* **2003**, *41*, 959–966.
(17) Kim, H.; Kim, M. G.; Shin, T. J.; Shin, H. J.; Cho, J. TiO_2@Sn core–shell nanotubes for fast and high density Li-ion storage material. *Electrochem. Commun.* **2008**, *10*, 1669–1672.
(18) Ren, J.; He, X.; Wang, L.; Pu, W.; Jiang, C.; Wan, C. Nanometer copper–tin alloy anode material for lithium-ion batteries. *Electrochim. Acta* **2007**, *52*, 2447–2452.
(19) Liu, S.; Yin, X.; Chen, L.; Li, Q.; Wang, T. Synthesis of self-assembled 3D flowerlike SnS_2 nanostructures with enhanced lithium ion storage property. *Solid State Sci.* **2010**, *12*, 712–718.
(20) Seo, J. W.; Jang, J. T.; Park, S. W.; Kim, C. J.; Park, B. W.; Cheon, J. W. Two-dimensional SnS_2 nanoplates with extraordinary high discharge capacity for lithium ion batteries. *Adv. Mater.* **2008**, *20*, 4269–4273.
(21) Kim, T. J.; Kim, C.; Son, D.; Choi, M.; Park, B. Novel SnS_2-nanosheet anodes for lithium-ion batteries. *J. Power Sources* **2007**, *167*, 529–535.

DOI: 10.1021/acs.accounts.7b00086
Acc. Chem. Res. XXXX, XXX, XXX–XXX

(22) Kim, H. S.; Chung, Y. H.; Kang, S. H.; Sung, Y. E. Electrochemical behavior of carbon-coated SnS_2 for use as the anode in lithium-ion batteries. *Electrochim. Acta* **2009**, *54*, 3606−3610.
(23) Lefebvre-Devos, I.; Olivier-Fourcade, J.; Jumas, J. C.; Lavela, P. Lithium insertion mechanism in SnS_2. *Phys. Rev. B: Condens. Matter Mater. Phys.* **2000**, *61*, 3110−3116.
(24) Patra, C. R.; Odani, A.; Pol, V. G.; Aurbach, D.; Gedanken, A. Microwave-assisted synthesis of tin sulfide nanoflakes and their electrochemical performance as Li-inserting materials. *J. Solid State Electrochem.* **2007**, *11*, 186−194.
(25) Courtney, I. A.; Dahn, J. R. Electrochemical and in situ X-ray diffraction studies of the reaction of lithium with tin oxide composites. *J. Electrochem. Soc.* **1997**, *144*, 2045−2052.
(26) Yang, Y.; Xie, C.; Ruffo, R.; Peng, H. L.; Kim, D. K.; Cui, Y. Single nanorod devices for battery diagnostics: a case study on $LiMn_2O_4$. *Nano Lett.* **2009**, *9*, 4109−4114.
(27) Raimann, P. R.; Hochgatterer, N. S.; Korepp, C.; Moller, K. C.; Winter, M.; Schrottner, H.; Hofer, F.; Besenhard, J. O. Monitoring dynamics of electrode reactions in Li-ion batteries by in situ ESEM. *Ionics* **2006**, *12*, 253−255.
(28) Zheng, H.; Rivest, J. B.; Miller, T. A.; Sadtler, B.; Lindenberg, A.; Toney, M. F.; Wang, L.-W.; Kisielowski, C.; Alivisatos, A. P. Observation of transient structural-transformation dynamics in a Cu_2S nanorod. *Science* **2011**, *333*, 206−209.
(29) Holmberg, V. C.; Panthani, M. G.; Korgel, B. A. Phase transitions, melting dynamics, and solid-state diffusion in a nano test tube. *Science* **2009**, *326*, 405−407.
(30) Zheng, H.; Smith, R. K.; Jun, Y.-w.; Kisielowski, C.; Dahmen, U.; Alivisatos, A. P. Observation of single colloidal platinum nanocrystal growth trajectories. *Science* **2009**, *324*, 1309−1312.
(31) Wang, F.; Yu, H.-C.; Chen, M.-H.; Wu, L.; Pereira, N.; Thornton, K.; Van der Ven, A.; Zhu, Y.; Amatucci, G. G.; Graetz, J. Tracking lithium transport and electrochemical reactions in nanoparticles. *Nat. Commun.* **2012**, *3*, 1201−1208.
(32) Huang, J. Y.; Zhong, L.; Wang, C. M.; Sullivan, J. P.; Xu, W.; Zhang, L. Q.; Mao, S. X.; Hudak, N. S.; Liu, X. H.; Subramanian, A.; Fan, H. Y.; Qi, L. A.; Kushima, A.; Li, J. In situ observation of the electrochemical lithiation of a single SnO_2 nanowire electrode. *Science* **2010**, *330*, 1515−1520.
(33) Gao, P.; Wang, L. P.; Zhang, Y. Y.; Huang, Y.; Liao, L.; Sutter, P.; Liu, K. H.; Yu, D. P.; Wang, E. G. High-resolution tracking asymmetric lithium insertion and extraction and local structure ordering in SnS_2. *Nano Lett.* **2016**, *16*, 5582−5588.
(34) Brousse, T.; Lee, S. M.; Pasquereau, L.; Defives, D.; Schleich, D. M. Composite negative electrodes for lithium ion cells. *Solid State Ionics* **1998**, *113*, 51−56.
(35) Stephenson, T.; Li, Z.; Olsen, B.; Mitlin, D. Lithium ion battery applications of molybdenum disulfide (MoS_2) nanocomposites. *Energy Environ. Sci.* **2014**, *7*, 209−231.
(36) Liu, Z.; Deng, H.; Mukherjee, P. Evaluating pristine and modified SnS_2 as a lithium-ion battery anode: a first-principles study. *ACS Appl. Mater. Interfaces* **2015**, *7*, 4000−4009.
(37) Jung, S. C.; Han, Y.-K. Lithium intercalation behaviors in Ge and Sn crystalline surfaces. *Phys. Chem. Chem. Phys.* **2013**, *15*, 13586−13592.

DOI: 10.1021/acs.accounts.7b00086
Acc. Chem. Res. XXXX, XXX, XXX−XXX